Available online at www.sciencedirect.com

ScienceDirect

Solid Earth Sciences 2 (2017) 43–54

www.elsevier.com/locate/SESCI

In situ boron isotopic analyses of tourmalines from Neogene magmatic rocks in the northern and southern margins of Tibet: Evidence for melting of continental crust and sediment recycling

Guo-Ning Gou [a,b], Qiang Wang [a,b,c,*], Derek A. Wyman [d], Xiao-Ping Xia [a], Gang-Jian Wei [a], Hai-Feng Guo [a]

[a] State Key Laboratory of Isotope Geochemistry, Guangzhou Institute of Geochemistry, Chinese Academy of Sciences, Guangzhou 510640, China
[b] University of Chinese Academy of Sciences, Beijing 100049, China
[c] CAS Center for Excellence in Tibetan Plateau Earth Sciences (CETES), Beijing 100101, China
[d] School of Geosciences, University of Sydney, NSW 2006, Australia

Received 22 January 2017; revised 3 March 2017; accepted 3 March 2017
Available online 8 April 2017

Abstract

Sediment recycling has important impacts on the differentiation of the continental crust, and is considered to mainly occur in arc settings. In collisional orogenic belts, however, sediment recycling processes are comparatively less well understood. In general, sedimentary rocks or tourmaline with continental affinities have boron (B) isotope compositions that differ from marine sedimentary rocks, magmatic rocks undergoing seawater alteration or tourmaline originating from these rocks or fluids. This study uses laser-ablation multi-collector, inductively coupled plasma-mass spectrometry (LA-MC-ICPMS) for in-situ B isotope analyses of tourmaline from the northern and southern margins of Tibet. Tourmalines from the Hudongliang Pliocene two mica rhyolites in the Songpan-Gangzi block and the Cuonadong Miocene two mica granites in the Himalayan Block have $\delta^{11}B$ values of $-10.47 \pm 0.54‰$ and $-12.48 \pm 1.04‰$, respectively. Combined with petrological and Nd–Sr isotope data, we suggest that these strongly peraluminous magmatic rocks from the northern and southern margins of Tibet were mainly generated by partial melting of subducted or overridden metasedimentary rocks with continental affinities due to the contraction caused by the collision between the Indian and Asian plates. Given the widespread occurrences of strongly peraluminous Neogene magmatic rocks in the southern and northern margin of Tibet, we suggest that the recycling of sediments with continental affinity played an important role in the evolution of continental crust during the collisional orogenic process.

Keywords: Tibet; Peraluminous magmatic rocks; Sediment recycling; In-situ B isotope; Tourmalines

1. Introduction

Sediment recycling has important impacts on the differentiation of the continental crust (Plank and Langmuir, 1993; Hawkesworth et al., 1997; Chauvel et al., 2008; Behn et al., 2011; Hacker et al., 2011; Liu and Rudnick, 2011; Marschall and Schumacher, 2012). Volcanic arc zones are commonly considered as the most important sites for the recycling of subducted marine sediments into the continental crust via arc magmatism (Kay, 1978; Plank and Langmuir, 1993; Hawkesworth et al., 1997; Shimoda et al., 1998; Chauvel et al., 2008; Behn et al., 2011). In collisional orogenic belts, however, except for element recycling (Cannaò et al., 2015) and fluid–rock interaction (Halama et al., 2014)

* Corresponding author. State Key Laboratory of Isotope Geochemistry, Guangzhou Institute of Geochemistry, Chinese Academy of Sciences, Guangzhou 510640, China.
E-mail address: wqiang@gig.ac.cn (Q. Wang).
Peer review under responsibility of Guangzhou Institute of Geochemistry.

http://dx.doi.org/10.1016/j.sesci.2017.03.003

in the Alps, sediment recycling processes have been comparatively less well understood.

Boron (B) is a quintessentially crustal element (Marschall and Jiang, 2011). Its average abundance in the mantle is relatively low, whereas rocks of the continental crust show relatively high average abundances, containing a large fraction of Earth's B budget (Dutrow and Henry, 2011; Chaussidon and Albarède, 1992). The primitive mantle had a relatively low $\delta^{11}B$ ($-10 \pm 2‰$) (Chaussidon and Marty, 1995). In general, marine sedimentary rocks and magmatic rocks undergoing seawater alteration, or tourmaline originating from these rocks or fluids, are enriched in ^{11}B but depleted in ^{10}B relative to the mantle and continental crust (Leeman and Sisson, 1996; Marschall et al., 2006; Marschall and Jiang, 2011). Consequently, relatively high $^{11}B/^{10}B$ ratios in rocks and minerals imply derivation of boron from average value of B in seawater, whereas lower $^{11}B/^{10}B$ ratio suggests a continental source of the boron (Marschall and Jiang, 2011). Therefore, this distinctive geochemical characteristic of B isotopes is widely used to assess several important geological processes, e.g., oceanic slab subduction or evolution of continental crust (e.g., Chaussidon and Albarède, 1992; Ishikawa and Nakamura, 1994; Bebout and Nakamura, 2003; Leeman and Sisson, 1996; Kasemann et al., 2000; Marschall and Jiang, 2011; Martin et al., 2016). For example, in volcanic arcs, continuous dehydration of micas from subducted slabs and boron transport via fluid into the mantle wedge is generally considered to have been responsible for the boron isotopic signature (e.g., Wunder et al., 2005).

As a borosilicate containing ~3 wt.% B, tourmaline has significant chemical variability because of the variety of sites in the structure and the ease with which several of these sites can incorporate a wide variety of chemical species (Hawthorne and Dirlam, 2011). Once formed, tourmaline is highly stable in a variety of rock types over an exceptionally large P–T range, extending from near surface conditions to pressures in the diamond stability field and to temperatures above 700 °C (Marschall et al., 2009a; Dutrow and Henry, 2011; Marschall and Jiang, 2011; Van Hinsberg et al., 2011a,b). Because of this compositional sensitivity, tourmaline is an excellent indicator of conditions in its host environment (Van Hinsberg et al., 2011a,b). With the development of in situ analytical techniques, in situ B isotopic analyses of tourmalines have been widely applied to provide valuable information on fluid–rock interaction, fluid or magma origin and evolution and the sources of ore deposits (e.g., Jiang and Palmer, 1998; Jiang et al., 1999, 2002, 2008; Marschall and Jiang, 2011; van Hinsberg et al., 2011a,b; Yang and Jiang, 2012).

Tourmaline is a very common mineral in peraluminous granites and rhyolites, which often occur in collisional orogenic belts, e.g., Himalayan–Tibetan Orogenic Belt. Neogene tourmaline-bearing two-mica granites occur widely in the Himalayan Block on the southern margin of the Tibetan Plateau (e.g., Le Fort et al., 1987; Inger and Harris, 1993; Harris and Massey, 1994; Guillot and Le Fort, 1995; Harris et al., 1995; Patiño Douce and Harris, 1998; Knesel and Davidson, 2002; Zhang et al., 2004, 2012; Liao et al., 2007; Guo and Wilson, 2012; Gao and Zeng, 2014; Liu et al., 2014, 2016a,b; Wu et al., 2015), but only minor Miocene–Quaternary tourmaline-bearing two-mica rhyolites are distributed along the northern margins of the Tibetan Plateau (Burchfiel et al., 1989; McKenna and Walker, 1990; Wang et al., 2012, 2016). Some researchers suggest that the leucogranites in the Himalayan Block crystallized from highly fractionated magmas, which originated from undetermined or weakly constrained sources, and underwent assimilation of crustal materials during their ascent (Wu et al., 2015; Liu et al., 2016a,b; Zheng et al., 2016). However, most researchers believe that these Neogene tourmaline-bearing two-mica granites or rhyolites on the northern and southern margins of the Himalayan–Tibetan Orogenic Belt were generated by dehydration melting of metasedimentary rocks involving biotite or muscovite or both (e.g., Le Fort et al., 1987; Burchfiel et al., 1989; McKenna and Walker, 1990; Inger and Harris, 1993; Harris and Massey, 1994; Guillot and Le Fort, 1995; Harris et al., 1995; Patiño Douce and Harris, 1998; Knesel and Davidson, 2002; Zhang et al., 2004, 2012; Liao et al., 2007; Guo and Wilson, 2012; Wang et al., 2012; Gao and Zeng, 2014). Therefore, the issue of source rock components needs to be further constrained. In particular, the question of whether the sedimentary rocks formed in either marine or continental settings, which has not ever been addressed before, needs to be resolved.

In this study, we undertook in-situ boron isotopic analyses of tourmalines from Neogene magmatic rocks in the northern and southern margins of Tibet in order to further constrain their source rock components.

2. Geological setting and sample characteristics

From South to North, the Tibetan Plateau mainly comprises the Himalaya, Lhasa, Qiangtang, and Songpan-Ganzi Blocks (Yin and Harrison, 2000; Chung et al., 2005) (Fig. 1a). The Himalayan Block lies between the Indian shield to the south and the Indus-Yalu suture to the north, and consists mainly of Precambrian–Mesozoic sedimentary and metasedimentary rocks with some Cambrian to Early Ordovician and Eocene–Miocene granites (Yin and Harrison, 2000; Zeng et al., 2011; Hou et al., 2012). The Songpan-Ganzi Block is bounded by the Jinshajiang suture to the south, and the Anyimaqen–Kunlun–Muztagh suture to the north (Yin and Harrison, 2000; Zeng et al., 2011; Hou et al., 2012; Guo and Wilson, 2012). The exposed Songpan-Ganzi Block consists mainly of Triassic and younger strata with some Early Mesozoic granites and Miocene–Quaternary volcanic lavas (Yin and Harrison, 2000; Weislogel et al., 2006; Ding et al., 2013; Zhang et al., 2014; Wang et al., 2005, 2011, 2012).

In this study, rock samples were collected from the Cuonadong Miocene (~16.7 Ma) tourmaline-bearing two-mica granites in the Himalayan Block (Yunnan, 2004) and ~3.0 Ma Hudongliang tourmaline-bearing two-mica rhyolites in the northern Hoh Xil area of the central Songpan-Gangzi Block (Wang et al., 2012), respectively (Fig. 1a–c). The Hudongliang tourmaline-bearing two mica rhyolites are located near

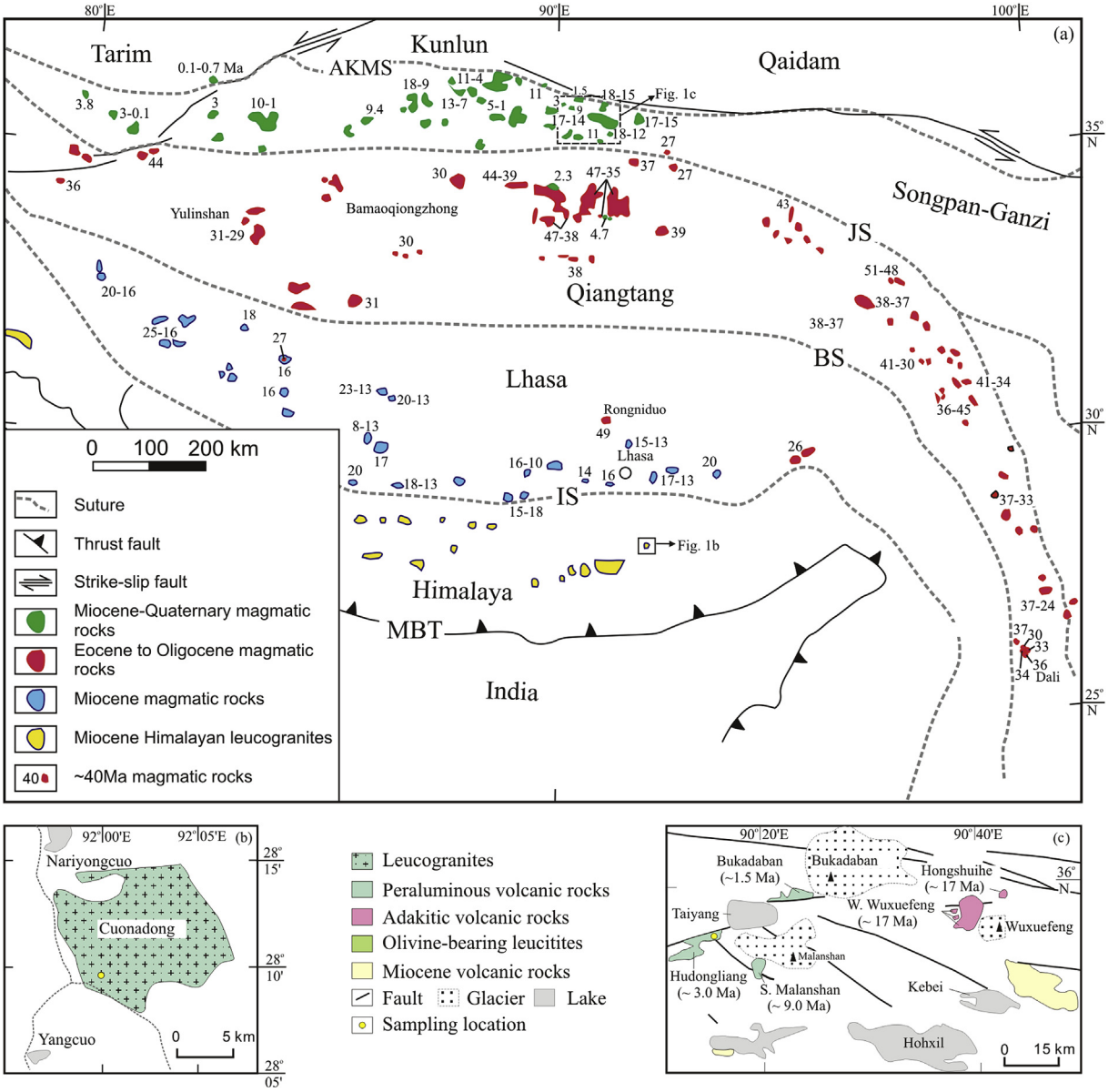

Fig. 1. (a) Sketch map of the Tibetan Plateau showing location and ages of magmatic bodies (after Yin and Harrison, 2000; Chung et al., 2005). (b–c) Geological map of the Cuonadong area in the Himalayan block and the Hoh Xil area of the Songpan-Ganzi block, showing the sampling locations. The age data are after Wang et al. (2008, 2010, 2012, 2016). AKMS—Anyimaqen–Kunlun–Muztagh; JS—Jinshajiang; BS—Bangong; IS—Indus.

Taiyang Lake (Fig. 1c), and contain potassium feldspar, albite, biotite, quartz, muscovite, and tourmaline phenocrysts, and similar microlitic minerals in the groundmass along with cryptocrystalline-glassy materials (Fig. 2a and b). The Cuonadong tourmaline-bearing two-mica granites are geographically located to the south of Nariyongcuo Lake (Fig. 1b), and consist of potassium feldspar, albite, biotite, quartz, muscovite, and tourmaline (Fig. 2c and d) and minor zircon and apatite. In the Cuonadong granites, tourmaline grains are in direct contact with potassium feldspar, plagioclase, and quartz (Fig. 2c and d), indicating that these four minerals most likely crystallized contemporaneously. All tourmaline grains, which are similar to the primitive tourmalines found in the crust-derived strongly peraluminous granites (London et al., 1996), occur as disseminated grains in both rhyolites and granites (Fig. 2a–d) in the studied areas, indicating that they crystallized directly from granitic magmas. Backscattered electronic images (Fig. 2e and f) indicate that tourmalines from both the rhyolites and granites have no compositional zoning and relatively homogeneous textures.

3. Analytical methods

Tourmaline grains of 0.1–1 mm in size were separated for each ca. 1 kg sample using standard density separation techniques. Tourmaline grains were handpicked and mounted in an epoxy resin disc, and then polished. Microscopic and back-scattered electron images were taken at the State Key

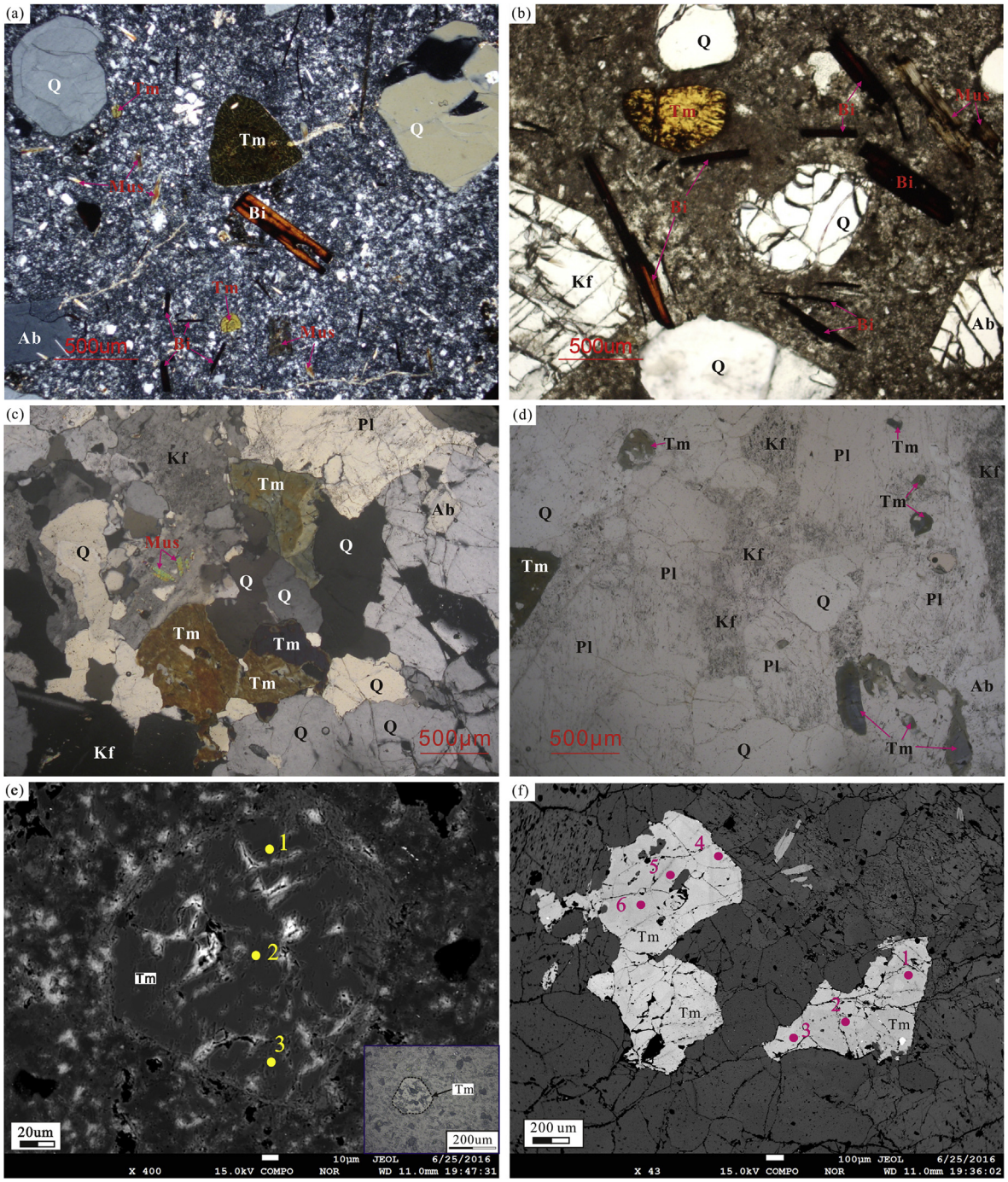

Fig. 2. Photomicrographs of the Hudongliang Pliocene two mica rhyolites in the Songpan-Gangzi block (a–b) and the Cuonadong Miocene two mica granites in the Himalayan Block (c–d). (a) Porphyry texture of the Hudongliang tourmaline-bearing two-mica rhyolite (sample $1P_2JD7-1$, crossed polarized light (xpl)). (b) Potassium feldspar, albite, quartz, muscovite, and tourmaline in the Hudongliang rhyolite (sample $1P_2JD7-1$, plane-polarized light (ppl)). (c) Potassium feldspar, plagioclase, albite, biotite, quartz, muscovite, and tourmaline in the Cuonadong Miocene two mica granites (sample 11SN36, xpl). (d) Potassium feldspar, plagioclase, albite, biotite, quartz, and tourmaline in the Cuonadong Miocene two mica granites (sample 11SN36, ppl). (e) Backscattered electronic image and analytical spots for major element compositions of tourmalines from the Hudongliang tourmaline-bearing two-mica rhyolite (sample $1P_2JD7-1$). 1, 2 and 3 are the analytical spots for the tourmaline compositions in Table 1. (f) Backscattered electron image and analytical spots for major element compositions of tourmalines from the Cuonadong Miocene two mica granites. 1, 2, 3, 4, 5 and 6 are the analytical spots for the tourmaline compositions in Table 1. Ab-albite; Bt-biotite; Kf-potassium feldspar, Mus-muscovite; Pl-plagioclase; Q-quartz; Tm-tourmaline, ppl-plane polarized light, xpl-cross polarized light.

Laboratory of Isotope Geochemistry, Guangzhou Institute of Geochemistry, Chinese Academy of Sciences (SKLaBIG GIG CAS) with a JEOL JXA-8100 Superprobe for inspecting internal morphology of individual tourmalines. Before B isotope analyses, the analyses for the compositions of the tourmaline grains were carried out at the SKLaBIG GIG CAS with a JEOL JXA-8100 Superprobe. Operating conditions were as the follows: 15 kV accelerating voltage, 20 nA beam current,

1–2 μm beam diameter, 10 s counting time and ZAF correction procedure for data reduction. The analytical procedures were described in detail in Huang et al. (2007). The mineral composition data are listed in Table 1.

Tourmaline in situ B isotope analyses were conducted on a Neptune Plus multicollector inductively coupled plasma mass spectrometer (MC-ICP-MS) and a matching RESOlution M-50 laser ablation system, at the SKLaBIG GIG CAS. The MC-ICPMS is fitted with a collector block containing 9 variable position Faraday cups and 8 Ion Counters (compact discrete dynamic multiplier, CDD or SEM). Detailed operating conditions (Table 2) for the laser ablation system and the MC-ICP-MS instrument and data reduction were approximately similar to those described by Hou et al. (2010), Míková et al. (2014), Guo et al. (2014) and Martin et al. (2015). The laser ablation system generated an ultraviolet laser of 193 nm. After laser homogenization, the energy was focused on the surfaces of samples with the laser output frequency of 5 Hz, and with an ablation diameter of 45 μm. During the analysis, both B isotope signals (L3: ^{10}B; H3: ^{11}B) were collected simultaneously by Faraday cups. The cup positions were adjusted and the masses were calibrated by using a 2 μg/mL H_3BO_3 solution (a product of Alfa Company) before connecting to the laser ablation system. The aerosol produced by laser ablation was blown out with He as the carrier gas, and after passing a T-cock, it was mixed with Ar gas and the mixture was injected into the plasma of the MC-ICP-MS for ionization. Before the analysis of samples, the instrumental parameters were optimized with IAEA B4 (a certified tourmaline reference for B isotopes from the International Atomic Energy Agency (Tonarini et al., 2003a)).

The data for *m/z* 10 and *m/z* 11 were collected simultaneously on L3 and H3 Faraday cups. Their on-peak-zero was measured for 27 s before the laser was on. After the laser was powered on, the measurements were taken in 400 cycles for each spot, and the integration time for each cycle was of 0.131 s. The $^{11}B/^{10}B$ of each spot was calculated after subtracting the on-peak zero on *m/z* 10 and *m/z* 11. Corrections for instrumental drift, mass bias between ^{10}B and ^{11}B were both conducted by a "standard-sample-standard" bracketing external standardization technique. One piece of standard tourmaline IAEA B4 with a size of ~3 × 3 × 2 mm was used for this purpose. Two spots on the IAEA B4 were measured before and after each 10 spots measurements of unknown samples, and the mass bias of the $^{11}B/^{10}B$ of the unknown samples were calibrated by reference to the mean of the four $^{11}B/^{10}B$ ratios of the IAEA B4 to its certificate value (Gonfiantini et al., 2003; Le Roux et al., 2004).

Off-line data reduction (including selection and integration of background and analyte signals) was performed by a spreadsheet program created in house by the authors. The time-resolved signal of single isotopes and isotope ratios was carefully inspected to verify the presence of perturbations related to inclusions, fractures and mixing of different sample domains. The final result of the B isotopic analyses is expressed in terms of $\delta^{11}B$, which is defined as follows: $\delta^{11}B$ (‰) = $[(^{11}B/^{10}B)_{Sample}/(^{11}B/^{10}B)_{Standard}-1] \times 1000$, where the standard was NIST SRM 951 boric acid from the National Institute of Standard Technology ($^{11}B/^{10}B_{NIST\ SRM\ 951}$ = 4.05003 (Ishikawa and Tera, 1997; Ishikawa et al., 2001). The internal precision for each spot after calculated into $\delta^{11}B$ was generally better than 0.1‰ (1σ).

Two international tourmaline reference standards (dravite (#108796) and schorl (#112566)) (Dyar et al., 2001; Leeman

Table 2
Detailed operating conditions for the laser ablation system and the MC-ICP-MS instrument.

Laser: RESOlution M-50	
Laser type	ArF Excimer
Wavelength	193 nm
Repetition rate	5 Hz
Crater size	44um
Ablation time	30 s
Carrier gas He flow rate	700 mL/min
Energy density (fluence) on target	4.0 J/cm^2
Pulse length	~20ns
Transport tubing	Nylon, 4 mm diameter; ~3 m length
ICP-MS: Neptune Plus	
Forward power	1250 W
Cool gas flow rate	14 L/min
Auxiliary gas flow rate	1.0 L/min
Carrier make up gas flow rate	0.98 L/min
Integration time	0.133 s
Data blocks collected	500

Table 1
The compositions for the tourmalines from Cenozoic magmatic rocks in Tibet.

Spots	SiO_2	TiO_2	Al_2O_3	FeO	MnO	MgO	CaO	Na_2O	K_2O	Cr_2O_3	NiO	Total
Sample 1P2JD7-1												
1	34.19	0.75	31.37	11.50	0.12	2.62	0.21	1.87	0.06	0.06	0.00	82.75
2	33.98	0.68	31.76	11.70	0.13	2.58	0.19	1.94	0.04	0.06	0.00	83.05
3	34.00	0.81	31.67	11.12	0.10	2.93	0.24	1.78	0.05	0.13	0.00	82.83
Sample 11SN36-6												
1	33.82	0.58	29.71	13.73	0.22	1.93	0.28	1.88	0.05	0.01	0.02	82.22
2	34.12	0.21	30.31	14.06	0.38	0.92	0.13	1.88	0.01	0.02	0.00	82.02
3	33.82	0.71	29.68	13.57	0.20	1.95	0.26	1.87	0.04	0.00	0.00	82.10
4	33.84	0.26	29.93	14.83	0.35	0.80	0.16	1.96	0.04	0.00	0.00	82.18
5	33.50	0.24	30.40	14.27	0.40	1.01	0.15	1.98	0.05	0.02	0.00	82.01
6	33.66	0.21	30.10	13.61	0.28	1.30	0.17	2.02	0.06	0.12	0.00	81.52

Table 3
Boron isotope compositions of series Boron isotope standards determined by LA-MC-ICP-MS.

Reference sample	Analyzed $\delta^{11}B$[a] value (2σ) (‰) in this study (n = 15[b])	Reference $\delta^{11}B$[a] value (2σ) (‰)	Reference
Dravite (#108796)	−6.89 ± 0.35	−6.6 ± 0.2	Dyar et al., 2001; Leeman and Tonarini, 2001
Schorl (#112566)	−13.21 ± 0.53	−12.50 ± 0.1	Dyar et al., 2001; Leeman and Tonarini, 2001
IMR RB1	−13.59 ± 0.43	−12.96 ± 0.97	Hou et al., 2010
IMR RB2	12.57 ± 0.35	−12.53 ± 0.57	Hou et al., 2010

[a] The values are the $\delta^{11}B$ (‰) values normalized to NIST SRM 951.
[b] The analyzed times (n) for Boron isotope standards are 15.

and Tonarini, 2001) and two laboratory tourmaline standards (IMR RB1 and IMR RB2) (Hou et al., 2010) were repeatedly measured along with the samples to monitor the quality of the measurements. The external precision of the $\delta^{11}B$ was generally better than ±0.5‰ (2 SD), and their values are all identical to the reported reference values within analytical errors (Table 3), demonstrating the reliably of the analytical procedure.

4. Analytical results

4.1. Mineral geochemistry

From core to rim (Fig. 2e; Table 1), the tourmalines from the Hudongliang rhyolites exhibit consistent SiO_2 (34.0–34.196 wt.%), Al_2O_3 (31.37–31.76 wt.%) and FeO (11.12–11.70 wt.%) and low MgO (2.58–2.93 wt.%), indicating homogeneous compositions. From core to rim (Fig. 2e; Table 1), the tourmalines from the Cuonadong granites exhibit consistent SiO_2 (33.50–34.12 wt.%) and Al_2O_3 (29.68–30.40 wt.%) and slightly variable and FeO (13.57–14.82 wt.%) and MgO (0.80–1.93 wt.%). Compared with the tourmalines from the Hudongliang rhyolites, the tourmalines from Cuonadong granites have relatively high FeO and low MgO contents, indicating some geochemical differences.

4.2. B isotope compositions of tourmalines

Tourmaline B isotopic data are listed in Table 4. 21 analyzed spots for tourmalines of the Hudongliang Pliocene two mica rhyolite sample ($1P_2JD7$-1) in the Songpan-Gangzi block exhibit homogeneous $^{11}B/^{10}B$ ratios ranging from 4.0054 to 4.0093 and consistent $\delta^{11}B$ values ranging from −11.03 to −10.06‰ (Table 4) with a mean of −10.47 ± 0.54‰ (Fig. 3a and b), which is in agreement with their homogeneous major element compositions from core to rim (Table 1; Fig. 2e). 35 analyzed spots for tourmalines of the Cuonadong Miocene two mica granite sample (11SN36) in the Himalayan Block also exhibit approximately

Table 4
LA-MC-ICPMS in-situ boron isotopic data on tourmaline from Neogene magmatic rocks from the northern and southern margins of Tibet.

Spots	$^{11}B/^{10}B$ ratios	$\delta^{11}B$ (‰)	1σ (‰)
Tourmaline from the Hudongliang pliocene two mica rhyolite sample ($1P_2J7D$) in northern Tibet			
$1P_2J7D$-1	4.0093	−10.06	0.10
$1P_2J7D$-2	4.0074	−10.54	0.09
$1P_2J7D$-3	4.0077	−10.45	0.08
$1P_2J7D$-4	4.0085	−10.24	0.11
$1P_2J7D$-5	4.0092	−10.08	0.08
$1P_2J7D$-6	4.0054	−11.03	0.10
$1P_2J7D$-7	4.0091	−10.11	0.12
$1P_2J7D$-8	4.0072	−10.57	0.09
$1P_2J7D$-9	4.0073	−10.56	0.10
$1P_2J7D$-10	4.0077	−10.45	0.10
$1P_2J7D$-11	4.0058	−10.93	0.08
$1P_2J7D$-12	4.0081	−10.34	0.12
$1P_2J7D$-13	4.0059	−10.89	0.08
$1P_2J7D$-14	4.0071	−10.59	0.08
$1P_2J7D$-15	4.0088	−10.18	0.07
$1P_2J7D$-16	4.0088	−10.19	0.09
$1P_2J7D$-17	4.0072	−10.58	0.09
$1P_2J7D$-18	4.0078	−10.43	0.10
$1P_2J7D$-19	4.0074	−10.52	0.09
$1P_2J7D$-20	4.0076	−10.47	0.08
$1P_2J7D$-21	4.0071	−10.59	0.07
Tourmaline from the Cuonadong Miocene two mica granite sample (11SN36) in southern Tibet			
11SN36-4-1	3.9991	−12.57	0.07
11SN36-4-2	3.9987	−12.68	0.08
11SN36-4-3	4.0006	−12.20	0.10
11SN36-4-4	4.0004	−12.26	0.10
11SN36-4-5	4.0015	−11.98	0.09
11SN36-4-6	3.9968	−13.13	0.08
11SN36-4-7	3.9991	−12.57	0.09
11SN36-4-8	3.9979	−12.86	0.09
11SN36-4-9	3.9961	−13.31	0.08
11SN36-4-10	3.9944	−13.73	0.07
11SN36-4-11	3.9995	−12.48	0.07
11SN36-4-12	3.9986	−12.69	0.08
11SN36-4-13	3.9975	−12.96	0.08
11SN36-4-14	3.9978	−12.89	0.11
11SN36-4-15	4.0007	−12.19	0.11
11SN36-4-16	4.0031	−11.60	0.09
11SN36-4-17	4.0025	−11.74	0.09
11SN36-4-18	3.9989	−12.62	0.11
11SN36-4-19	4.0005	−12.23	0.08
11SN36-4-20	3.9997	−12.43	0.13
11SN36-4-21	3.9992	−12.55	0.10
11SN36-4-22	4.0023	−11.78	0.10
11SN36-4-23	4.0016	−11.96	0.11
11SN36-4-24	4.0040	−11.36	0.09
11SN36-4-25	4.0017	−11.92	0.09
11SN36-4-26	4.0030	−11.62	0.09
11SN36-4-27	3.9993	−12.52	0.11
11SN36-4-28	4.0006	−12.20	0.10
11SN36-4-29	4.0003	−12.27	0.11
11SN36-4-30	4.0018	−11.90	0.11
11SN36-4-31	3.9984	−12.74	0.09
11SN36-4-32	3.9995	−12.48	0.11
11SN36-4-33	3.9989	−12.62	0.08
11SN36-4-34	3.9972	−13.05	0.09
11SN36-4-35	3.9982	−12.81	0.10

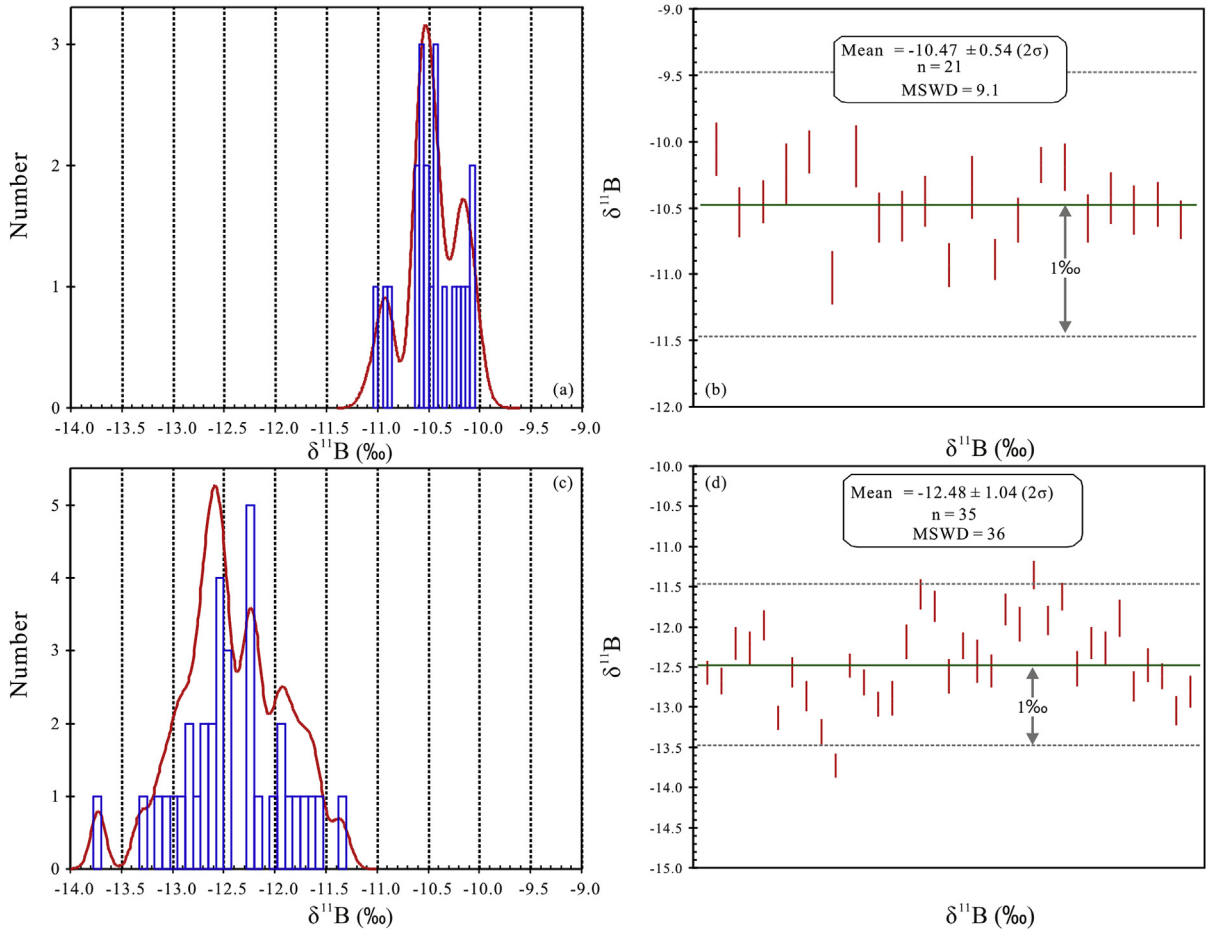

Fig. 3. $\delta^{11}B$ mean values of tourmalines from the Hudongliang two mica rhyolites (a–b) and the Cuonadong two mica granites (c–d).

homogeneous $^{11}B/^{10}B$ ratios ranging from 3.9944 to 4.0040 and consistent $\delta^{11}B$ values ranging from −13.73 to −11.36‰ (Table 4) with a mean of −12.48 ± 1.04‰ (Fig. 3c and d). Therefore, the tourmalines from the Hudongliang rhyolites exhibit slightly higher $\delta^{11}B$ values than the tourmalines from the Cuonandong two mica granites (Table 4 and Fig. 3a and c), which is in agreement with their homogeneous major element compositions from core to rim (Table 1; Fig. 2f).

5. Discussion

Boron isotope fractionation between tourmaline, aqueous fluid and granitic melt is a highly controversial topic that has received much discussion in the literature (e.g., Palmer et al., 1992; Jiang and Palmer, 1998; Hervig et al., 2002; Tonarini et al., 2003b; Meyer et al., 2008; Trumbull et al., 2008; Marschall et al., 2009b; London, 2011; Marschall and Jiang, 2011). Based on studies on volcanic glasses, Tonarini et al. (2003b) suggest that B isotope fractionation is mostly related to the relative amount of trigonal and tetrahedral boron sites in the glass network rather than to other processes, including the speciation of hydrous species in the glass structure. A basic consensus is that the nature and extent of isotopic fractionation between tourmaline and fluids is different from that between tourmaline and melts (Leeman and Sisson, 1996; Marschall and Jiang, 2011). Trigonally co-ordinated $B(OH)_3$ is the only significant species that occurs in a solution or fluid due to their low pH (Palmer et al., 1992), but B generally occurs as tetrahedral co-ordinated $B(OH)_4^-$ in a melt (Jiang and Palmer, 1998). In general, ^{11}B is preferentially partitioned into aqueous fluids during heating and decomposition of hydrous minerals (clay minerals and white mica) or during fluid–rock interaction (e.g., Jiang and Palmer, 1998; Marschall and Jiang, 2011). Thus, tourmaline directly crystallizing from a fluid has higher $\delta^{11}B$ values than the clays and micas from which the fluid originated (Marschall and Jiang, 2011). However, if granitic tourmaline crystallized directly from a melt, there should be relatively little isotopic fractionation as the change in the boron symmetry during tourmaline crystallization is small; i.e., the $\delta^{11}B$ values of granitic tourmalines would be similar to those of the melt (Jiang and Palmer, 1998).

In this study, petrographic characteristics (Fig. 2a–d) suggest that the tourmalines from the Hudongliang and Cuonadong Neogene magmatic rocks directly crystallized from felsic magmas, and their $\delta^{11}B$ values should be similar to those of the magmas. The tourmalines of the Hudongliang Pliocene two mica rhyolite sample ($1P_2JD7$-1) have a mean $\delta^{11}B$ value of −10.47 ± 0.54‰, which is consistent with those (−9.71 ± 0.04) of whole rock sample ($1P_2JD7$-1) within the

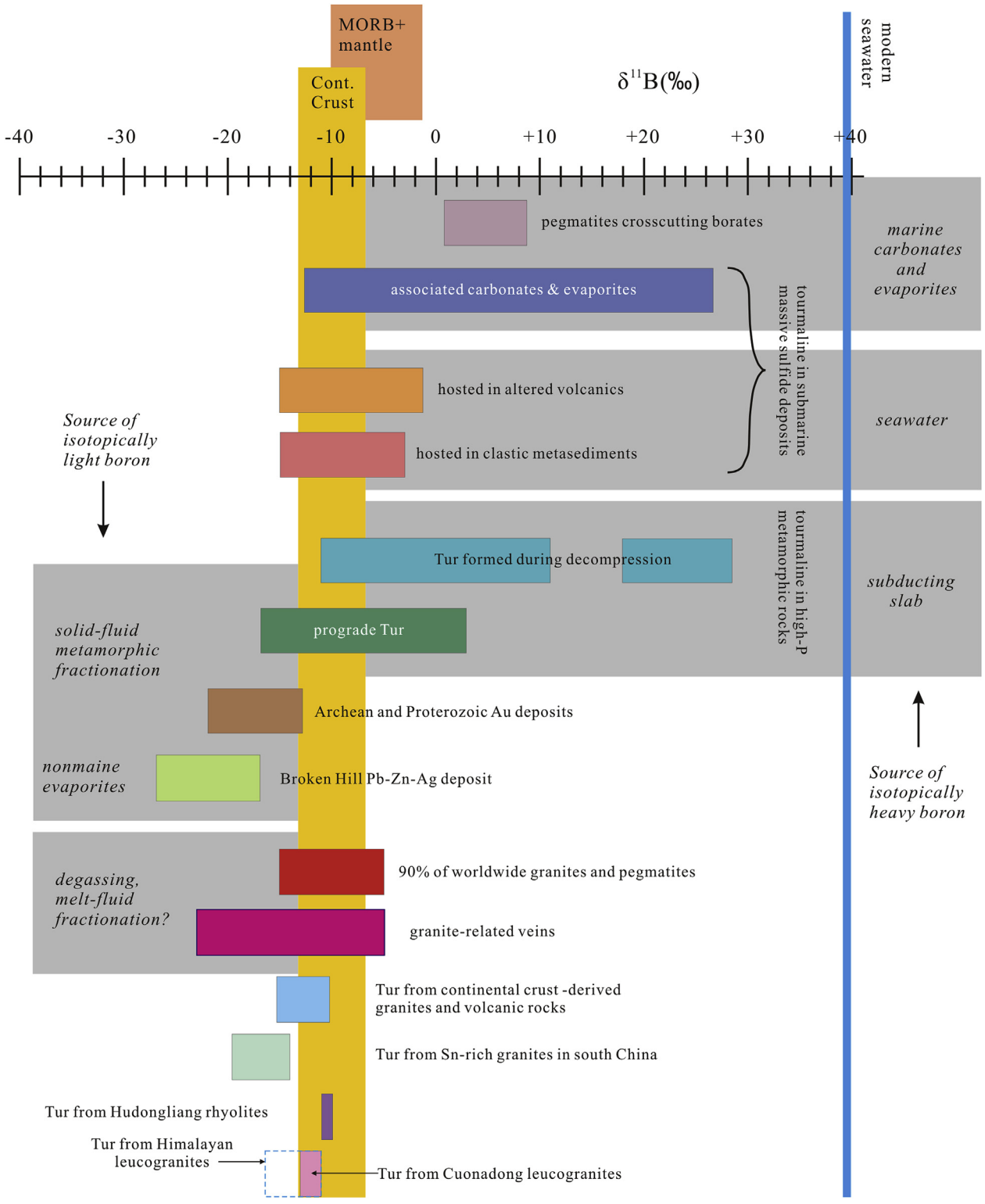

Fig. 4. Measured B isotope composition as a function of host rock type (colored boxes) and inferred B sources (grey bands) (after Marschall and Jiang (2011)). Isotopically heavy B (= high $\delta^{11}B$ value) is ultimately sourced from seawater and may enter a rock via fluids or melts derived from a subducting slab or from carbonate or evaporite sequences in the crust, or directly from seawater circulating through the rocks. Isotopically light B (= low $\delta^{11}B$ value) is typically sourced from nonmarine evaporites or produced by isotopic fractionation between solids and fluids during metamorphic dehydration (Marschall and Jiang, 2011). Tur = tourmaline; MORB = mid-ocean ridge basalt. The range of whole-rock $\delta^{11}B$ values of the Himalayan leucogranites is from Jiang et al. (2003). The $\delta^{11}B$ value range for tourmalines from the Himalayan leucogranites is from Chaussidon and Albarède (1992) and Yang et al. (2015).

range of errors (Wang et al., unpublished data). The tourmalines from the Cuonadong Miocene two mica granite sample (11SN36) in the Himalayan Block have a mean $\delta^{11}B$ value of −12.48 ± 1.04‰, which is in the range of tourmaline $\delta^{11}B$ values (−16.3 to −10.3‰) of the Himalayan leucogranites (Chaussidon and Albarède, 1992; Yang et al., 2015) (Fig. 4).

The $\delta^{11}B$ values of granitic tourmalines were commonly considered to be similar to those of the melt (Jiang and Palmer, 1998; Jiang et al., 2008; Talikka and Vuori, 2010; Zhao et al., 2011; Yang and Jiang, 2012; Yang et al., 2015). The tourmalines of both the Hudongliang rhyolites and Cuonandong granites have $\delta^{11}B$ values ranging from −12.48 to −10.47‰, which are clearly lower than those (>0 in general) of marine sedimentary rocks or magmatic rocks undergoing seawater alteration or tourmalines from above rocks or fluids from them (Fig. 4) (Marschall and Jiang, 2011). E.g., the metasomatic tourmaline owing to influx of hydrous fluids released from the subducted oceanic slab in the Syros Island has exceptionally high $\delta^{11}B$ (+18 to +28‰) (Marschall et al., 2006). However, their $\delta^{11}B$ values are similar to those (−10.3 to −15.4‰) of magmatic tourmalines from continental crust-derived granites and volcanic rocks (Fig. 4) (Jiang, 2001; Jiang et al., 2008; Talikka and Vuori, 2010; Zhao et al., 2011; Yang and Jiang, 2012; Guo et al., 2014; Yang et al., 2015), and very close to those (−10 ± 3‰) of average continental crust (Fig. 4) (Marschall and Jiang, 2011). Alternatively, some other studies have suggested that the $\delta^{11}B$ values of tourmaline may be higher than those of melt (e.g., Macgregor et al., 2013), which would imply that the melts of both the Hudongliang rhyolites and Cuonandong granites had $\delta^{11}B$ values lower than −12.48 to −10.47‰. In other words, both the Hudongliang rhyolites and Cuonandong granites may have had crustal sources with lower $\delta^{11}B$ values than those of the tourmalines or the (−10 ± 3‰) average continental crust (Fig. 4) (Marschall and Jiang, 2011).

Miocene–Pliocene peraluminous lavas including the Hudongliang rhyolites in the Songpan-Ganzi block have higher εNd (−5.8 to −8.6) and lower $^{87}Sr/^{86}Sr$ (0.7125–0.7178) (McKenna and Walker, 1990; Wang et al., 2012; Zhang et al., 2012) than the respective values (−13.0 to −20.0 and 0.7256 to 0.8547) for Late Oligocene–Miocene leucogranites, including the Cuonandong granites in the Himalayan block (e.g., Inger and Harris, 1993; Harris and Massey, 1994; Guillot and Le Fort, 1995; Harris et al., 1995; Knesel and Davidson, 2002; Zhang et al., 2004; Liao et al., 2007; Guo and Wilson, 2012; Gao and Zeng, 2014; Liu et al., 2014; Wu et al., 2015). This indicates that Neogene peraluminous rocks in the northern and southern margins of Tibet were generated by partial melting of metasedimentary rocks with different components. Petrological and Sr–Nd isotopic data also suggest, however, that they were both most likely derived from Precambrian–Mesozoic metasedimentary rocks (e.g., metapelites or metagreywackes) on the northern and southern margins of Tibet, respectively (e.g., Le Fort et al., 1987; Burchfiel et al., 1989; McKenna and Walker, 1990; Inger and Harris, 1993; Harris and Massey, 1994; Guillot and Le Fort, 1995; Harris et al., 1995; Patiño Douce and Harris, 1998; Knesel and Davidson, 2002; Zhang et al., 2004, 2012; Liao et al., 2007; Guo and Wilson, 2012; Wang et al., 2012; Gao and Zeng, 2014; Liu et al., 2014; Wu et al., 2015). The question of whether their source rocks were sedimentary rocks formed in marine or continental settings has been more difficult to resolve. Our new results demonstrate that the Hudongliang rhyolites and Cuonandong granites exhibit tourmaline $\delta^{11}B$ values close to those of average continental crust or continental crust-derived granites (Fig. 4), indicating that they were mainly generated by partial melting of the metasedimentary rocks with continental affinities. Moreover, these source rocks were most probably subducted or overridden in the northern and southern margins of Tibet during contraction associated with the collision of the Indian plate with the Asian plate (Yin and Harrison, 2000; Tapponnier et al., 2001; Ding et al., 2003; Kapp et al., 2003, 2005).

Traditionally, volcanic arcs are considered to be the most important sites for the recycling of subducted marine sediments into the continental crust via arc magmatism (Kay, 1978; Plank and Langmuir, 1993; Hawkesworth et al., 1997; Shimoda et al., 1998; Chauvel et al., 2008; Behn et al., 2011). Given the widespread occurrences of Neogene peraluminous magmatic rocks in the southern and northern margin of Tibet, however, we suggest that the recycling of sediments with continental affinity played an important role in the formation of these peraluminous magmatic rocks and the evolution of continental crust during the collisional orogenic process.

Acknowledgment

We would like to thank Editor-in-Chief Professor Wei-Dong Sun, and an anonymous reviewer for their constructive and helpful reviews. We also thank Professor J.G. Liou and Dr. M. Satish-Kumar for their suggestions on the early edition of this paper. We appreciate the assistance of Dr. Kejun Hou for providing us with standard tourmalines IAEA B4 and IMR RB2 and Professor Zhongyuan Ren for in situ B isotopic analyzing. Financial support for this research was provided by the DREAM Program of China (No. 2016YFC0600407), the Strategic Priority Research Program (B) of the Chinese Academy of Sciences (grant no. XDB03010600), the Key Program of the Chinese Academy of Sciences (QYZDJ-SSW-DQC026), the National Natural Science Foundation of China (Nos. 41630208 and 41421062), talent project of Guangdong Province (2014TX01Z079), and GIGCAS 135 project 135TP201601. This is contribution No. IS-2371 from GIGCAS.

References

Bebout, G.E., Nakamura, E., 2003. Record in metamorphic tourmalines of subduction-zone devolatilization and boron cycling. Geology 31 (5), 407–410.

Behn, M.D., Kelemen, P.B., Hirth, G., Hacker, B.R., Massonne, H.-J., 2011. Diapirs as the source of the sediment signature in arc lavas. Nat. Geosci. 4 (9), 641–646.

Burchfiel, B.C., Molnar, P., Zhao, Z., Liang, K.U., Wang, S., Huang, M., Sutter, J., 1989. Geology of the Ulugh Muztagh area, northern Tibet. Earth Planet. Sci. Lett. 94 (1–2), 57–70.

Cannaò, E., Agostini, S., Scambelluri, M., Tonarini, S., Godard, M., 2015. B, Sr and Pb isotope geochemistry of high-pressure Alpine metaperidotites monitors fluid-mediated element recycling during serpentinite dehydration in subduction mélange (Cima di Gagnone, Swiss Central Alps). Geochim. Cosmochim. Acta 163, 80−100.

Chaussidon, M., Albarède, F., 1992. Secular boron isotope variations in the continental crust: an ion microprobe study. Earth Planet. Sci. Lett. 108 (4), 229−241.

Chaussidon, M., Marty, B., 1995. Primitive boron isotope composition of the mantle. Science 269, 383−386.

Chauvel, C., Lewin, E., Carpentier, M., Arndt, N.T., Marini, J.-C., 2008. Role of recycled oceanic basalt and sediment in generating the Hf-Nd mantle array. Nat. Geosci. 1 (1), 64−67.

Chung, S.-L., Chu, M.-F., Zhang, Y., Xie, Y., Lo, C.-H., Lee, T.-Y., Lan, C.-Y., Li, X., Zhang, Q., Wang, Y., 2005. Tibetan tectonic evolution inferred from spatial and temporal variations in post-collisional magmatism. Earth Sci. Rev. 68 (3−4), 173−196.

Ding, L., Kapp, P., Zhong, D., Deng, W., 2003. Cenozoic volcanism in Tibet: evidence for a transition from oceanic to continental subduction. J. Petrol. 44 (10), 1833−1865.

Ding, L., Yang, D., Cai, F.L., Pullen, A., Kapp, P., Gehrels, G.E., Zhang, L.Y., Zhang, Q.H., Lai, Q.Z., Yue, Y.H., Shi, R.D., 2013. Provenance analysis of the Mesozoic Hoh-Xil-Songpan-Ganzi turbidites in northern Tibet: implications for the tectonic evolution of the eastern Paleo-Tethys Ocean. Tectonics 32 (1), 34−48.

Dutrow, B.L., Henry, D.J., 2011. Tourmaline: a geologic DVD. Elements 7 (5), 301−306.

Dyar, M.D., Wiedenbeck, M., Robertson, D., Cross, L.R., Delaney, J.S., Ferguson, K., Francis, C.A., Grew, E.S., Guidotti, C.V., Hervig, R.L., Hughes, J.M., Husler, J., Leeman, W., Mcguire, A.V., Rhede, D., Rothe, H., Paul, R.L., Richards, I., Yates, M., 2001. Reference ,minerals for the microanalysis of light elements. Geostand. Newsl. 25 (2−3), 441−463.

Gao, L.-E., Zeng, L., 2014. Fluxed melting of metapelite and the formation of Miocene high-CaO two-mica granites in the Malashan gneiss dome, southern Tibet. Geochim. Cosmochim. Acta 130 (0), 136−155.

Gonfiantini, R., Tonarini, S., Gröning, M., Adorni-Braccesi, A., Al-Ammar, A.S., Astner, M., Bächler, S., Barnes, R.M., Bassett, R.L., Cocherie, A., Deyhle, A., Dini, A., Ferrara, G., Gaillardet, J., Grimm, J., Guerrot, C., Krähenbühl, U., Layne, G., Lemarchand, D., Meixner, A., Northington, D.J., Pennisi, M., Reitznerová, E., Rodushkin, I., Sugiura, N., Surberg, R., Tonn, S., Wiedenbeck, M., Wunderli, S., Xiao, Y., Zack, T., 2003. Intercomparison of boron isotope and concentration measurements. Part II: evaluation of results. Geostand. Newsl. 27, 41−57.

Guillot, S., Le Fort, P., 1995. Geochemical constraints on the bimodal origin of High Himalayan leucogranites. Lithos 35 (3−4), 221−234.

Guo, H.-F., Xia, X.-P., Wei, G.-J., Wang, Q., Zhao, Z.-H., Huang, X.-L., Zhang, H.-X., Yuan, C., Li, Wu-X., 2014. LA-MC-ICPMS in-situ boron isotope analyses of tourmalines from the Shangbao granites (southern Hunan Province) and its geological significance. Geochemica 43 (1), 11−19 (in Chinese with English abstract).

Guo, Z.F., Wilson, M., 2012. The Himalayan leucogranites: constraints on the nature of their crustal source region and geodynamic setting. Gondwana Res. 22 (2), 360−376.

Hacker, B.R., Kelemen, P.B., Behn, M.D., 2011. Differentiation of the continental crust by relamination. Earth Planet. Sci. Lett. 307 (3−4), 501−516.

Halama, R., Konrad-Schmolke, M., Sudo, M., Marschall, H.R., Wiedenbeck, M., 2014. Effects of fluid−rock interaction on $^{40}Ar/^{39}Ar$ geochronology in high-pressure rocks (Sesia-Lanzo Zone, Western Alps). Geochim. Cosmochim. Acta 126, 475−494.

Harris, N., Massey, J., 1994. Decompression and anatexis of Himalayan metapelites. Tectonics 13 (6), 1537−1546.

Harris, N., Ayres, M., Massey, J., 1995. Geochemistry of granitic melts produced during the incongruent melting of muscovite: implications for the extraction of Himalayan leucogranitic magmas. J. Geophys. Res. 100, 15,767−15,777.

Hawkesworth, C.J., Turner, S.P., Mcdermott, F., Peate, D.W., Van Calsteren, P., 1997. U-Th isotopes in arc magmas: implications for element transfer from subducted crust. Science 276, 561−565.

Hawthorne, F.C., Dirlam, D.M., 2011. Tourmaline the indicator mineral: from atomic arrangement to viking navigation. Elements 7 (5), 307−312.

Hervig, R.L., Moore, G.M., Williams, L.B., Peacock, S.M., Holloway, J. r., Roggensack, K., 2002. Isotopic and elemental partitioning of boron between hydrous fluid and silicate melt. Am. Mineral. 87, 769−774.

Hou, K.J., Li, Y.H., Xiao, Y.K., Liu, F., Tian, Y.R., 2010. In situ boron isotope measurements of natural geological materials by LA-MC-ICP-MS. Chin. Sci. Bull. 55 (29), 3305−3311.

Hou, Z.-Q., Zheng, Y.-C., Zeng, L.-S., Gao, L.-E., Huang, K.-X., Li, W., Li, Q.-Y., Fu, Q., Liang, W., Sun, Q.-Z., 2012. Eocene-Oligocene granitoids in southern Tibet: constraints on crustal anatexis and tectonic evolution of the Himalayan orogen. Earth Planet. Sci. Lett. 349−350, 38−52.

Huang, X.L., Xu, Y.G., Lo, C.H., Wang, R.C., Lin, C.Y., 2007. Exsolution lamellae in a clinopyroxene megacryst aggregate from Cenozoic Basalt, Leizhou Peninsula, South China: petrography and chemical evolution. Contrib. Mineral. Petrol. 154, 691−705.

Inger, S., Harris, N., 1993. Geochemical constraints on leucogranite magmatism in the Langtang Valley, Nepal Himalaya. J. Petrol. 34 (2), 345−368.

Ishikawa, T., Nakamura, E., 1994. Origin of the slab component in arc lavas form across-arc variation of B and Pb isotopes. Nature 370, 205−208.

Ishikawa, T., Tera, F., 1997. Source, composition and distribution of the fluid in the Kurile mantle wedge: constraints from across-arc variations of B/Nb and B isotopes. Earth Planet. Sci. Lett. 152 (1−4), 123−138.

Ishikawa, T., Tera, F., Nakazawa, T., 2001. Boron isotope and trace element systematics of the three volcanic zones in the Kamchatka arc. Geochim. Cosmochim. Acta 65, 4523−4537.

Jiang, S.-Y., Palmer, M.R., Slack, J.F., Shaw, D.R., 1999. Boron isotope systematics of tourmaline formation in the Sullivan Pb-Zn-Ag deposit, British Columbia, Canada. Chem. Geol. 158 (1−2), 131−144.

Jiang, S.-Y., Palmer, M.R., 1998. Boron isotope systematics of tourmaline from granites and pegmatites; a synthesis. Eur. J. Mineral. 10 (6), 1253−1265.

Jiang, S.-Y., 2001. Boron isotope geochemistry of hydrothermal ore deposits in China: a preliminary study. Phys. Chem. Earth Part A Solid Earth Geodesy 26 (9−10), 851−858.

Jiang, S.-Y., Palmer, M.R., Yeats, C.J., 2002. Chemical and boron isotopic compositions of tourmaline from the Archean Big Bell and Mount Gibson gold deposits, Murchison Province, Yilgarn Craton, Western Australia. Chem. Geol. 188 (3−4), 229−247.

Jiang, S.Y., Yang, J.H., Novak, M., Selway, J., 2003. Chemical and boron isotopic compositions of tourmaline from the Lavicky leucogranite, Czech Republic. Geochem. J. 37, 545−556.

Jiang, S.-Y., Radvanec, M., Nakamura, E., Palmer, M., Kobayashi, K., Zhao, H.-X., Zhao, K.-D., 2008. Chemical and boron isotopic variations of tourmaline in the Hnilec granite-related hydrothermal system, Slovakia: constraints on magmatic and metamorphic fluid evolution. Lithos 106 (1−2), 1−11.

Kapp, P., Murphy, M.A., Yin, A., Harrison, T.M., Ding, L., Guo, J., 2003. Mesozoic and Cenozoic tectonic evolution of the Shiquanhe area of western Tibet. Tectonics 22, 1029. http://dx.doi.org/10.1029/2001TC001332.

Kapp, P., Yin, A., Harrison, T.M., Ding, L., 2005. Cretaceous-Tertiary shortening, basin development, and volcanism in central Tibet. Geol. Soc. Am. Bull. 117 (7−8), 865−878.

Kasemann, S., Erzinger, J., Franz, G., 2000. Boron recycling in the continental crust of the central Andes from the Palaeozoic to Mesozoic, NW Argentina. Contrib. Mineral. Petrol. 140 (3), 328−343.

Kay, R.W., 1978. Aleutian magnesian andesites-melts from subducted Pacific ocean crust. J. Volcanol. Geotherm. Res. 4, 117−132.

Knesel, K.M., Davidson, J.P., 2002. Insights into collisional magmatism from isotopic fingerprints of melting reactions. Science 296 (5576), 2206−2208.

Leeman, W.P., Sisson, V.B., 1996. Geochemistry of boron and its implications for crustal and mantle processes. Boron: mineralogy, petrology and geochemistry. In: Grew, E.S., Anovitz, L.M. (Eds.), Reviews in Mineralogy, vol. 33, pp. 645−708.

Leeman, W.P., Tonarini, S., 2001. Boron isotopic analysis of proposed borosilicate mineral reference samples. Geostand. Newsl. 25, 399−403.

Le Fort, P., Cuney, M., Deniel, C., France-Lanord, C., Sheppard, S.M.F., Upreti, B.N., Vidal, P., 1987. Crustal generation of the Himalayan leucogranites. Tectonophysics 134 (1−3), 39−57.

Le Roux, P.J., Shirey, S.B., Benton, L., Hauri, E.H., Mock, T.D., 2004. In situ, multiple-multiplier, laser ablation ICP-MS measurement of boron isotopic composition ($\delta^{11}B$) at the nanogram level. Chem. Geol. 203 (1−2), 123−138.

Liao, Z., Mo, X., Pan, G., Zhu, D., Wang, L., Jiang, X., Zhao, Z., 2007. Spatial and temporal distribution of peraluminous granites in Tibet and their tectonic significance. J. Asian Earth Sci. 29 (2−3), 378−389.

Liu, X.-M., Rudnick, R.L., 2011. Constraints on continental crustal mass loss via chemical weathering using lithium and its isotopes. Proc. Natl. Acad. Sci. U. S. A. 108 (52), 20873−20880.

Liu, Z.-C., Wu, F.-Y., Ji, W.-Q., Wang, J.-G., Liu, C.-Z., 2014. Petrogenesis of the Ramba leucogranite in the Tethyan Himalaya and constraints on the channel flow model. Lithos 208−209 (0), 118−136.

Liu, Z.-C., Wu, F.-Y., Ding, L., Liu, X.-C., Wang, J.-G., Ji, W.-Q., 2016a. Highly fractionated Late Eocene (~35 Ma) leucogranite in the Xiaru Dome, Tethyan Himalaya, South Tibet. Lithos 240−243, 337−354.

Liu, X.-C., Wu, F.-Y., Yu, L.-J., Liu, Z.-C., Ji, W.-Q., Wang, J.-G., 2016b. Emplacement age of leucogranite in the Kampa Dome, southern Tibet. Tectonophysics 667, 163−175.

London, D., Morgan, G.B., Wolf, M.B., 1996. Boron in granitic rocks and their contact aureoles. Rev. Mineral. 33, 299−330.

London, D., 2011. Experimental synthesis and stability of tourmaline: a historical overview. Can. Mineral. 49, 117−136.

Macgregor, J., Grew, E.S., De Hoog, J.C.M., Harley, S.L., Kowalski, P.M., Yates, M.G., Carson, C.J., 2013. Boron isotopic composition of tourmaline, prismatine, and grandidierite from granulite facies paragneisses in the Larsemann Hills, Prydz Bay, East Antarctica: evidence for a non-marine evaporite source. Geochim. Cosmochim. Acta 123, 261−283.

Marschall, H.R., Ludwig, T., Altherr, R., Kalt, A., Tonarini, S., 2006. Syros metasomatic tourmaline: evidence for very high-d^{11}B fluids in subduction zones. J. Petrol. 47, 1915−1942.

Marschall, H.R., Meyer, C., Wunder, B., Ludwig, T., Heinrich, W., 2009b. Experimental boron isotope fractionation between tourmaline and fluid: confirmation from in situ analyses by secondary ion mass spectrometry and from Rayleigh fractionation modelling. Contrib. Mineral. Petrol. 158, 675−681.

Marschall, H.R., Jiang, S.-Y., 2011. Tourmaline isotopes: no element left behind. Elements 7 (5), 313−319.

Marschall, H.R., Schumacher, J.C., 2012. Arc magmas sourced from melange diapirs in subduction zones. Nat. Geosci. 5 (12), 862−867.

Marschall, H.R., Storey, C., Dhuime, B., Leat, P., Hawkesworth, C., 2009a. Archaean-proterozoic evolution in East Antarctica. Geochim. Cosmochim. Acta 73 (13), A837.

Martin, C., Ponzevera, E., Harlow, G., 2015. In situ lithium and boron isotope determinations in mica, pyroxene, and serpentine by LA-MC-ICP-MS. Chem. Geol. 412, 107−116.

Martin, C., Flores, K.E., Harlow, G.E., 2016. Boron isotopic discrimination for subduction-related serpentinites. Geology 44, 899−902.

McKenna, L.W., Walker, J.D., 1990. Geochemistry of crustally derived leucocratic igneous rocks from the Ulugh Muztagh area, northern Tibet and their implications for the formation of the Tibetan Plateau. J. Geophys. Res. 95 (B13), 21483−21502.

Meyer, C., Wunder, B., Meixner, A., Romer, R.L., Heinrich, W., 2008. Boron-isotope fractionation between tourmaline and fluid: an experimental re-investigation. Contrib. Mineral. Petrol. 156, 259−267.

Míková, J., Kosler, J., Wiedenbeck, M., 2014. Matrix effects during laser ablation MC ICP-MS analysis of boron isotopes in tourmaline. J. Anal. Atomic Spectrom. 29, 903−914.

Palmer, M.R., London, D., Morgan, G.B., Babb, H.A., 1992. Experimental determination of fractionation of 11B/10B between tourmaline and aqueous vapour: a temperature and pressure dependent isotopic system. Chem. Geol. (Isotope Geosci. Sect.) 101, 123−130.

Patiño Douce, A.E., Harris, N., 1998. Experimental constraints on Himalayan anatexis. J. Petrol. 39, 689−710.

Plank, T., Langmuir, C.H., 1993. Tracing trace elements from sediment input to volcanic output at subduction zones. Nature 362, 739−743.

Shimoda, G., Tatsumi, Y., Nohda, S., Ishizaka, K., Jahn, B.M., 1998. Setouchi high-Mg andesites revisited: geochemical evidence for melting of subducting sediments. Earth Planet. Sci. Lett. 160 (3−4), 479−492.

Talikka, M., Vuori, S., 2010. Geochemical and boron isotopic compositions of tourmalines from selected gold-mineralised and barren rocks in SW Finland. Bull. Geol. Soc. Finl. 82, 113−128.

Tapponnier, P., Xu, Z., Roger, F., Meyer, B., Arnaud, N., Wittlinger, G., Yang, J., 2001. Oblique stepwise rise and growth of the Tibet Plateau. Science 294 (5547), 1671−1677.

Trumbull, R.B., Krienitz, M.S., Gottesmann, B., Wiedenbeck, M., 2008. Chemical and boron-isotope variations in tourmalines from an S-type granite and its source rocks: the Erongo granite and tourmalinites in the Damara Belt, Namibia. Contrib. Mineral. Petrol. 155, 1−18.

Tonarini, S., Pennisi, M., Adorni-Braccesi, A., Dini, A., Ferrara, G., Gonfiantini, R., Wiedenbeck, M., Gröning, M., 2003a. Intercomparison of boron isotope and concentration measurements. Part I: selection, preparation and homogeneity tests of the intercomparison materials. Geostand. Geoanal. Res. 2003 (27), 21−39.

Tonarini, S., Forte, C., Petrini, R., Ferrara, G., 2003b. Melt/biotite $^{11}B/^{10}B$ isotopic fractionation and the boron local environment in the structure of volcanic glasses. Geochim. Cosmochim. Acta 67, 1863−1873.

Van Hinsberg, V.J., Henry, D.J., Dutrow, B.L., 2011a. Tourmaline as a petrologic forensic mineral: a unique recorder of its geologic past. Elements 7 (5), 327−332.

Van Hinsberg, V.J., Henry, D.J., Marschall, H.R., 2011b. Tourmaline: an ideal indicator of its host environment. Can. Mineral. 49 (1), 1−16.

Wang, Q., Mcdermott, F., Xu, J.-F., Bellon, H., Zhu, Y.-T., 2005. Cenozoic K-rich adakitic volcanic rocks in the Hohxil area, northern Tibet: lower-crustal melting in an intracontinental setting. Geology 33 (6), 465−468.

Wang, Q., Wyman, D.A., Xu, J.F., Dong, Y.H., Vasconcelos, P.M., Pearson, N., Wan, Y.S., Dong, H., Li, C.F., Yu, Y.S., Zhu, T.X., Feng, X.T., Zhang, Q.Y., Zi, F., Chu, Z.Y., 2008. Eocene melting of subducting continental crust and early uplifting of central Tibet: evidence from central-western Qiangtang high-K calc-alkaline andesites, dacites and rhyolites. Earth Planet. Sci. Lett. 272, 158−171.

Wang, Q., Wyman, D.A., Li, Z.X., Sun, W.D., Chung, S.L., Vasconcelos, P.M., Zhang, Q.Y., Dong, H., Yu, Y.S., Pearson, N., Qiu, H.N., Zhu, T.X., Feng, X.T., 2010. Eocene north-south trending dikes in central Tibet: new constraints on the timing of east-west extension with implications for early plateau uplift? Earth Planet. Sci. Lett. 298, 205−216.

Wang, Q., Li, Z.-X., Chung, S.-L., Wyman, D.A., Sun, Y.-L., Zhao, Z.-H., Zhu, Y.-T., Qiu, H.-N., 2011. Late Triassic high-Mg andesite/dacite suites from northern Hohxil, North Tibet: geochronology, geochemical characteristics, petrogenetic processes and tectonic implications. Lithos 126 (1−2), 54−67.

Wang, Q., Chung, S.-L., Li, X.-H., Wyman, D., Li, Z.-X., Sun, W.-D., Qiu, H.-N., Liu, Y.-S., Zhu, Y.-T., 2012. Crustal melting and flow beneath Northern Tibet: evidence from mid-Miocene to Quaternary strongly peraluminous rhyolites in the southern Kunlun range. J. Petrol. 53 (12), 2523−2566.

Wang, Q., Hawkesworth, C.J., Wyman, D., Chung, S.-L., Wu, F.-Y., Li, X.-H., Li, Z.-X., Gou, G.-N., Zhang, X.-Z., Tang, G.-J., Dan, W., Ma, L., Dong, Y.-H., 2016. Pliocene-Quaternary crustal melting in central and northern Tibet and insights into crustal flow. Nat. Commun. 7, 11888. http://dx.doi.org/10.1038/ncomms11888.

Weislogel, A.L., Graham, S.A., Chang, E.Z., Wooden, J.L., Gehrels, G.E., Yang, H., 2006. Detrital zircon provenance of the late Triassic Songpan-Ganzi complex: sedimentary record of collision of the North and South China blocks. Geology 34, 97−100.

Wunder, B., Meixner, A., Romer, R.L., Wirth, R., Heinrich, W., 2005. The geochemical cycle of boron: constraints from boron isotope partitioning experiments between mica and fluid. Lithos 84 (3−4), 206−216.

Wu, F.Y., Liu, Z.C., Liu, X.C., Ji, W.Q., 2015. Himalayan leucogranite: petrogenesis and implications to orogenesis and plateau uplift. Acta Petrol. Sin. 31 (1), 1−36.

Yang, S.-Y., Jiang, S.-Y., 2012. Chemical and boron isotopic composition of tourmaline in the Xiangshan volcanic-intrusive complex, Southeast China:

evidence for boron mobilization and infiltration during magmatic-hydrothermal processes. Chem. Geol. 312−313 (0), 177−189.

Yang, S.-Y., Jiang, S.-Y., Palmer, M.R., 2015. Chemical and boron isotopic compositions of tourmaline from the Nyalam leucogranites, South Tibetan Himalaya: implication for their formation from B-rich melt to hydrothermal fluids. Chem. Geol. 419, 102−113.

Yin, A., Harrison, T.M., 2000. Geologic evolution of the Himalayan-Tibetan orogen. Annu. Rev. Earth Planet. Sci. 28, 211−280.

Yunnan Geoological Survey Institute (Yunnan), 2004. 1:250000 Longzixian (H46c004002) regional geological survey in Tibet.

Zeng, L., Gao, L.-E., Xie, K., Liu-Zeng, J., 2011. Mid-Eocene high Sr/Y granites in the Northern Himalayan Gneiss Domes: melting thickened lower continental crust. Earth Planet. Sci. Lett. 303 (3−4), 251−266.

Zhang, H., Harris, N., Parrish, R., Kelley, S., Zhang, L., Rogers, N., Argles, T., King, J., 2004. Causes and consequences of protracted melting of the mid-crust exposed in the North Himalayan antiform. Earth Planet. Sci. Lett. 228 (1−2), 195−212.

Zhang, L.Y., Ding, L., Yang, D., Xu, Q., Cai, F.L., Liu, D.L., 2012. Origin of middle Miocene leucogranites and rhyolites on the Tibetan Plateau: constraints on the timing of crustal thickening and uplift of its northern boundary. Sci. Bull. 57 (5), 511−524.

Zhang, L.-Y., Ding, L., Pullen, A., Xu, Q., Liu, D.-L., Cai, F.-L., Yue, Y.-H., Lai, Q.-Z., Shi, R.-D., Ducea, M.N., Kapp, P., Chapman, A., 2014. Age and geochemistry of western Hoh-Xil-Songpan-Ganzi granitoids, northern Tibet: implications for the Mesozoic closure of the Paleo-Tethys ocean. Lithos 190−191 (0), 328−348.

Zhao, K.-D., Jiang, S.-Y., Nakamura, E., Moriguti, T., Palmer, M.R., Yang, S.-Y., Dai, B.-Z., Jiang, Y.-H., 2011. Fluid-rock interaction in the Qitianling granite and associated tin deposits, South China: evidence from boron and oxygen isotopes. Ore Geol. Rev. 43, 243−248.

Zheng, Y.-C., Hou, Z.-Q., Fu, Q., Zhu, D.-C., Liang, W., Xu, P., 2016. Mantle inputs to Himalayan anatexis: insights from petrogenesis of the Miocene Langkazi leucogranite and its dioritic enclaves. Lithos 264, 125−140.